Alexandria Engineering Journal (2015) 54, 713–723

HOSTED BY
ELSEVIER

Alexandria University
Alexandria Engineering Journal
www.elsevier.com/locate/aej
www.sciencedirect.com

ORIGINAL ARTICLE

Navier–Stokes flow in converging–diverging distensible tubes

Taha Sochi

University College London, Department of Physics & Astronomy, Gower Street, London WC1E 6BT, United Kingdom

Received 1 July 2014; revised 12 March 2015; accepted 31 March 2015
Available online 27 April 2015

KEYWORDS
1D flow;
Navier–Stokes;
Distensible tubes;
Converging–diverging tubes;
Irregular conduits;
Non-linear systems

Abstract We use a method based on the lubrication approximation in conjunction with a residual-based mass-continuity iterative solution scheme to compute the flow rate and pressure field in distensible converging–diverging tubes for Navier–Stokes fluids. We employ an analytical formula derived from a one-dimensional version of the Navier–Stokes equations to describe the underlying flow model that provides the residual function. This formula correlates the flow rate to the boundary pressures in straight cylindrical elastic tubes with constant-radius. We validate our findings by the convergence toward a final solution with fine discretization as well as by comparison to the Poiseuille-type flow in its convergence toward analytic solutions found earlier in rigid converging–diverging tubes. We also tested the method on limiting special cases of cylindrical elastic tubes with constant-radius where the numerical solutions converged to the expected analytical solutions. The distensible model has also been endorsed by its convergence toward the rigid Poiseuille-type model with increasing the tube wall stiffness. Lubrication-based one-dimensional finite element method was also used for verification. In this investigation five converging–diverging geometries are used for demonstration, validation and as prototypes for modeling converging–diverging geometries in general.

1. Introduction

The flow of fluids in converging–diverging tubes has many scientific, technological and medical applications such as transportation in porous media, filtration processes, polymer processing, and pathological stenoses and aneurysms [1–13]. There are many studies about the flow in converging–diverging rigid conduits [14–21] and distensible conduits with fixed cross sections [22–28] separately as well as many other different geometries and fluid and conduit mechanical properties [29–31]. There is also a considerable number of studies on the flow in converging–diverging distensible conduits; although large part of which is related to medical applications such as stenosis and blood flow modeling [32–42].

Several methods have been used in the past for investigating and modeling the flow in distensible converging–diverging geometries; the majority are based on the numerical discretization methods such as finite element and spectral methods although other approaches such as stochastic techniques have also been employed. However, due to the huge difficulties associating this subject which combines tube wall deformability with convergence–divergence non-linearities, most of these

E-mail address: t.sochi@ucl.ac.uk
Peer review under responsibility of Faculty of Engineering, Alexandria University.

http://dx.doi.org/10.1016/j.aej.2015.03.028
1110-0168 © 2015 Faculty of Engineering, Alexandria University. Production and hosting by Elsevier B.V.

Nomenclature

α	correction factor for axial momentum flux	p	pressure
β	stiffness coefficient in the pressure-area relation	$\mathbf{p}$	pressure vector
κ	viscosity friction coefficient	p_i	inlet pressure
μ	fluid dynamic viscosity	p_o	outlet pressure
ν	fluid kinematic viscosity	Δp	pressure drop
ρ	fluid mass density	$\Delta\mathbf{p}$	pressure perturbation vector
ς	Poisson's ratio of tube wall	Q	volumetric flow rate
A	tube cross-sectional area at actual pressure	Q_a	analytic flow rate for rigid tube
A_{in}	tube cross-sectional area at inlet	Q_e	numeric flow rate for elastic tube
A_o	tube cross-sectional area at reference pressure	Q_r	numeric flow rate for rigid tube
A_{ou}	tube cross-sectional area at outlet	$\mathbf{r}$	residual vector
E	Young's elastic modulus of the tube wall	R	tube radius
f	flow continuity residual function	R_{max}	maximum unstressed tube radius
h_o	tube wall thickness at reference pressure	R_{min}	minimum unstressed tube radius
$\mathbf{J}$	Jacobian matrix	t	time
L	tube length	x	tube axial coordinate (inlet at $x = 0$ and outlet at $x = L$)
N	number of discretized tube nodes		

studies are based on substantial approximations and modeling compromises. Moreover, they are usually based on very complex mathematical and computational infrastructures which are not only difficult to implement and use but also difficult to verify and validate. Also, some of these methods, such as stochastic techniques, are computationally demanding and hence they may be prohibitive in some cases. Therefore, simple, reliable and computationally low cost techniques are highly desirable where analytical solutions are not available due to excessive difficulties or even impossibility of obtaining such solutions which is the case in most circumstances.

In this paper we propose the use of the lubrication approximation with a residual-based non-linear solution scheme in association with an analytical expression for the flow of Navier–Stokes fluids in straight cylindrical elastic tubes with fixed radius to obtain the flow rate and pressure field in a number of cylindrically-symmetric converging–diverging geometries with elastic wall mechanical properties. The proposed method combines simplicity, robustness and ease of implementation. Moreover, it produces solutions which are very close to any targeted analytical solutions as the convergence behavior in the investigated special cases reveals.

Although the proposed method is related to a single distensible tube, it can also be extended to a network of interconnected distensible tubes with partially or totally converging–diverging conduits by integrating these conduits into the network and giving them a special treatment based on the proposed method. This approach, can be utilized for example in modeling stenoses and other types of flow conduits with irregular geometries as part of fluid flow networks in the hemodynamic and hemorheologic studies and in the filtration investigations.

The method also has a wider validity domain than what may be thought initially with regard to the deformability characteristics. Despite the fact that in this paper we use a single analytical expression correlating the flow rate to the boundary pressures for a distensible tube with elastic mechanical properties, the method can be well adapted to other types of mechanical characteristics, such as tubes with viscoelastic wall rheology, where different pressure-area constitutive relations do apply. In fact there is no need even to have an analytical solution for the underlying flow model that provides the basic flow characterization for the discretized elements of the converging–diverging geometries in the lubrication approximation. What is actually needed is only a well defined flow relation: analytical, or empirical, or even numerical [43] as long as it is viable to find the flow in the discretized elements of the lubrication ensemble using such a relation to correlate the flow rate to the boundary pressures.

There is also no need for the geometry to be of a fixed or regular shape as long as a characteristic flow can be obtained on the discretized elements, and hence the method can be applied not only to axi-symmetric geometries with constant-shape and varying cross-sectional area in the flow direction but can also be extended to non-symmetric geometries with irregular and varying shape along the flow direction if the flow in the deformable discretized elements can be characterized by a well-defined flow relation. The method can as well be applied to non-straight flow conduits with and without regular or varying cross-sectional shapes such as bending compliant pipes.

2. Method

The flow of Navier–Stokes fluids in a cylindrical tube with a cross-sectional area A and length L assuming a slip-free incompressible laminar axi-symmetric flow with negligible gravitational body forces and fixed velocity profile is described by the following one-dimensional system of mass continuity and linear momentum conservation principles

$$\frac{\partial A}{\partial t} + \frac{\partial Q}{\partial x} = 0 \quad t \geqslant 0, \ \ x \in [0, L] \tag{1}$$

$$\frac{\partial Q}{\partial t} + \frac{\partial}{\partial x}\left(\frac{\alpha Q^2}{A}\right) + \frac{A}{\rho}\frac{\partial p}{\partial x} + \kappa\frac{Q}{A} = 0 \quad t \geqslant 0, \ \ x \in [0, L] \tag{2}$$

In these two equations, Q is the volumetric flow rate, t is the time, x is the axial coordinate along the tube length, α is the momentum flux correction factor, ρ is the fluid mass density, p is the axial pressure which is a function of the axial coordinate, and κ is the viscosity friction coefficient which is usually given by $\kappa = \frac{2\pi\alpha\nu}{\alpha-1}$ where ν is the fluid kinematic viscosity defined as the ratio of the fluid dynamic viscosity μ to its mass density [44–46,27,47,48,21]. These relations are usually supported by a constitutive relation that correlates the pressure to the cross-sectional area in a distensible tube, to close the system in the three variables A, Q and p and hence provide a complete mathematical description for the flow in such conduits.

The correlation between the local pressure and cross-sectional area in a compliant tube can be described by many mathematical constitutive relations depending on the mechanical characterization of the tube wall and its response to pressure such as being elastic or viscoelastic, and linear or non-linear. The following is a commonly used pressure-area constitutive elastic relation that describes such a dependency

$$p = \frac{\beta}{A_o}\left(\sqrt{A} - \sqrt{A_o}\right) \tag{3}$$

where β is the tube wall stiffness coefficient which is usually defined by

$$\beta = \frac{\sqrt{\pi} h_o E}{1 - \varsigma^2} \tag{4}$$

A_o is the reference cross-sectional area corresponding to the reference pressure which in this equation is set to zero for convenience without affecting the generality of the results, A is the tube cross-sectional area at the actual pressure p as opposite to the reference pressure, h_o is the tube wall thickness at the reference pressure, while E and ς are respectively the Young's elastic modulus and Poisson's ratio of the tube wall. The essence of Eq. (3) is that the pressure is proportional to the radius growth with a proportionality stiffness coefficient that is scaled by the reference area. It should be remarked that we assume here a constant ambient transmural pressure along the axial direction which is set to zero and hence the reference cross-sectional area represents unstressed state where A_o is constant along the axial direction.

Based on the pressure-area relation of Eq. (3), and using the one-dimensional Navier–Stokes system of Eqs. (1) and (2) for the time-independent flow by dropping the time terms, the following equation correlating the flow rate Q to the inlet and outlet boundary areas of an elastic cylindrical tube with a constant unstressed cross-sectional area over its axial direction can be obtained

$$Q = \frac{-\kappa L + \sqrt{\kappa^2 L^2 + \frac{4\alpha\beta}{5\rho A_o}\ln\left(A_{in}/A_{ou}\right)\left(A_{in}^{5/2} - A_{ou}^{5/2}\right)}}{2\alpha \ln\left(A_{in}/A_{ou}\right)} \tag{5}$$

where A_{in} and A_{ou} are the tube cross-sectional area at the inlet and outlet respectively such that $A_{in} > A_{ou}$. This relation, which in essence correlates the flow rate to the boundary pressures, has been previously [28] derived and validated by a finite element scheme. As will be explained later on, Eq. (5) is used in conjunction with Eq. (7) to characterize the flow in the discretized sections of the tube.

The residual-based lubrication approach, which is proposed in the present paper to find the pressure field and flow rate in converging–diverging distensible tubes, starts by discretizing the tube in the axial direction into ring-like elements. Each one of these elements is approximated as a single tube with a constant radius, which averages the inlet and outlet radii of the element, to which Eq. (5) applies. A system of non-linear equations based on the mass continuity residual and boundary conditions is then formed.

For a tube discretized into $(N-1)$ elements, there are N nodes: two boundaries and $(N-2)$ interior nodes. Each one of these nodes has a well-defined axial pressure value according to the one-dimensional formulation. Also for the interior nodes, and due to the incompressibility of the flow, the total sum of the volumetric flow rate, signed $(+/-)$ according to its direction with respect to the node, is zero due to the absence of sources and sinks, and hence $(N-2)$ residual functions which describe the net flow at the interior nodes can be formed. This is associated with two given boundary conditions for the inlet and outlet boundary nodes to form N equations.

A standard method for solving such a system is to use an iterative non-linear simultaneous solution scheme such as Newton–Raphson method where an initial guess for the interior nodal pressures is proposed and used in conjunction with the Jacobian matrix of the system to find the pressure perturbation vector which is then used to adjust the pressure values and repeat this process until a convergence criterion based on the size of the residual norm is reached. The process is based on iterative solving of the following equation

$$\mathbf{J}\Delta\mathbf{p} = -\mathbf{r} \tag{6}$$

where $\mathbf{J}$ is the Jacobian matrix, $\mathbf{p}$ is the vector of variables which represent the pressure values at the boundary and interior nodes, and $\mathbf{r}$ is the vector of residuals which, for the interior nodes, is based on the continuity of the volumetric flow rate as given by

$$f_j = \sum_{i=1}^{m} Q_i = 0 \tag{7}$$

where m is the number of discretized elements connected to node j which is two in this case, and Q_i is the signed volumetric flow rate in element i as characterized by Eq. (5). Eq. (6) is then solved in each iteration for $\Delta\mathbf{p}$ which is then used to update $\mathbf{p}$. The convergence will be declared when the norm of the residual vector, $\mathbf{r}$, becomes within a predefined error tolerance. In fact Eq. (6) is the result of a linearization scheme where the components of the matrix equation are defined by Eq. (7). More details about this solution scheme can be found in [27,11].

3. Implementation and results

The proposed residual-based lubrication method was implemented in a computer code and flow solutions were obtained for an extensive range of fluid, flow and tube characterizations such as fluid viscosity, flow profile, and tube mechanical properties. Five regular converging–diverging axi-symmetric tube geometries were used in the current investigation; representative graphic images of these geometries are shown in Fig. 1, while the mathematical relations that describe the dependency of the tube radius, R, on the tube axial coordinate, x, for these geometries are given in Table 1. A generic converging–diverging tube profile demonstrating the setting

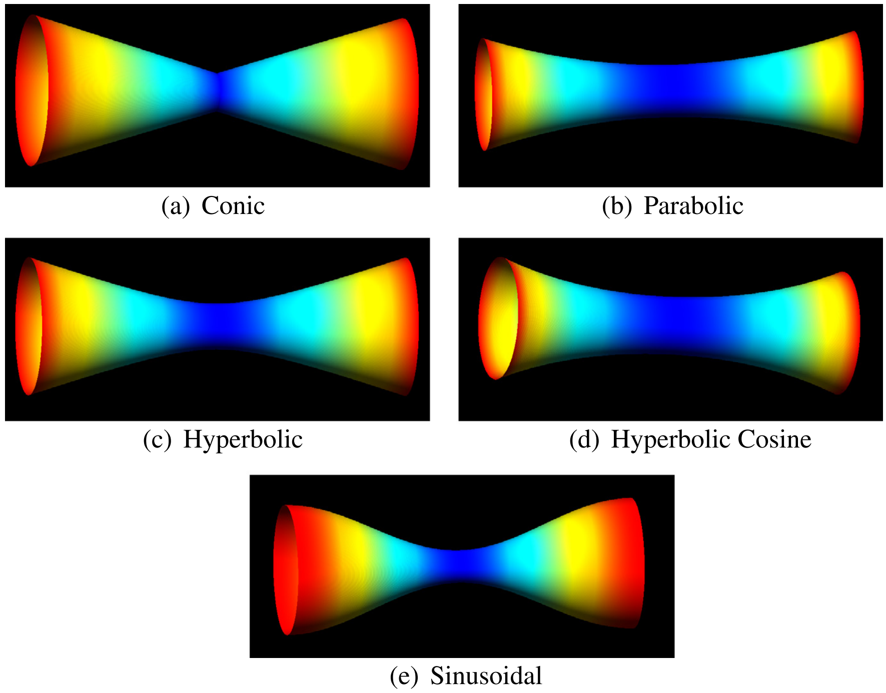

Fig. 1 Converging–diverging tube geometries used in the current investigation.

Table 1 The equations describing the dependency of the tube radius R on the tube axial coordinate x for the five converging–diverging geometries used in the current investigation. In all these relations $-\frac{L}{2} \leqslant x \leqslant \frac{L}{2}$ and $R_{min} < R_{max}$ where R_{min} is the tube minimum radius at $x = 0$ and R_{max} is the tube maximum radius at $x = \pm\frac{L}{2}$ as demonstrated in Fig. 2.

Geometry	$R(x)$
Conic	$R_{min} + \frac{2(R_{max}-R_{min})}{L}\lvert x\rvert$
Parabolic	$R_{min} + \left(\frac{2}{L}\right)^2 (R_{max} - R_{min})x^2$
Hyperbolic	$\sqrt{R_{min}^2 + \left(\frac{2}{L}\right)^2 (R_{max}^2 - R_{min}^2)x^2}$
Hyperbolic cosine	$R_{min} \cosh\left[\frac{2}{L} \operatorname{arccosh}\left(\frac{R_{max}}{R_{min}}\right)x\right]$
Sinusoidal	$\left(\frac{R_{max}+R_{min}}{2}\right) - \left(\frac{R_{max}-R_{min}}{2}\right)\cos\left(\frac{2\pi x}{L}\right)$

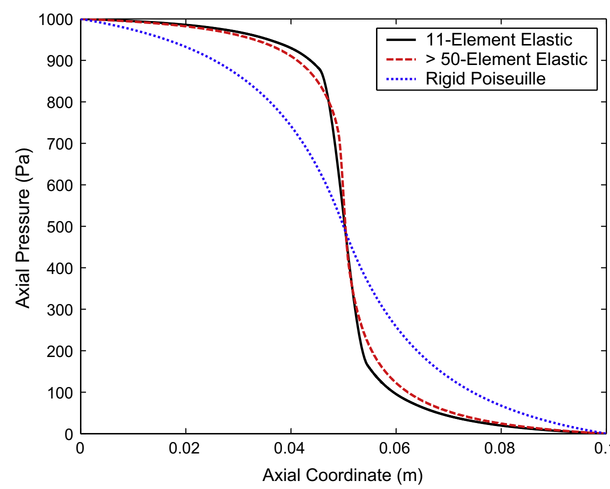

Fig. 3 Axial pressure as a function of axial coordinate for a converging–diverging elastic tube with conic geometry having $L = 0.1$ m, $R_{min} = 0.005$ m, $R_{max} = 0.01$ m, and $\beta = 236.3$ Pa m. The fluid properties are: $\rho = 1000$ kg m^{-3} and $\mu = 0.01$ Pa s while the inlet and outlet pressures are: $p_i = 1000$ Pa and $p_o = 0.0$ Pa. The Poiseuille-type flow uses a rigid tube with the same unstressed geometry and the same μ and boundary pressures. The converged flow rate for the elastic Navier–Stokes and rigid Poiseuille-type flows are respectively: $Q_e = 0.000255889$ m^3 s^{-1} and $Q_r = 0.000842805$ m^3 s^{-1} while the analytic flow rate for the rigid tube as obtained from the first equation in Table 2 is $Q_a = 0.000841498$ m^3 s^{-1}.

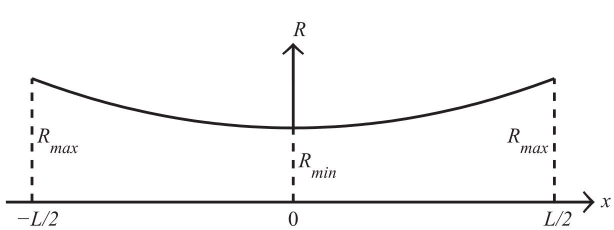

Fig. 2 Generic converging–diverging tube profile demonstrating the coordinate system setting for the correlation between the axial coordinate x and the tube radius R used in Table 1.

of the coordinate system for the R–x correlation, as used in Table 1, is shown in Fig. 2. These geometries have been used previously [20,21] to find flow relations for Newtonian and power law fluids in rigid tubes. A representative sample of the flow solutions on distensible converging–diverging tubes are also given in Figs. 3–7.

In all flow simulations, including the ones shown in Figs. 3–7, we used a range of evenly-divided discretization meshes to

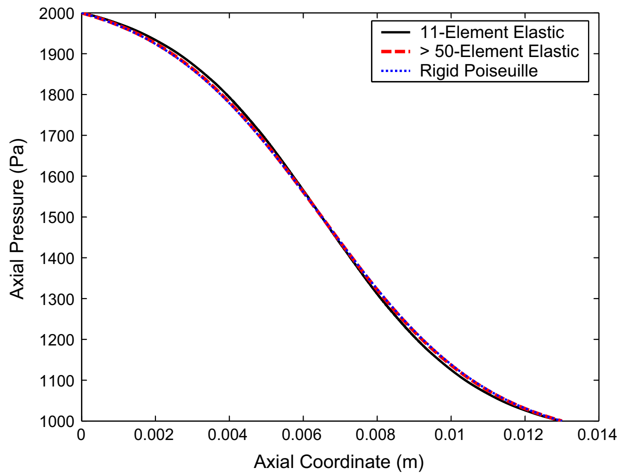

Fig. 4 Axial pressure as a function of axial coordinate for a converging–diverging elastic tube with parabolic geometry having $L = 0.013$ m, $R_{min} = 0.0017$ m, $R_{max} = 0.0025$ m, and $\beta = 28059.0$ Pa m. The fluid properties are: $\rho = 1100$ kg m^{-3} and $\mu = 0.006$ Pa s while the inlet and outlet pressures are: $p_i = 2000$ Pa and $p_o = 1000$ Pa. The Poiseuille-type flow uses a rigid tube with the same unstressed geometry and the same μ and boundary pressures. The converged flow rate for the elastic Navier–Stokes and rigid Poiseuille-type flows are respectively: $Q_e = 6.58209 \times 10^{-5}$ m^3 s^{-1} and $Q_r = 6.62929 \times 10^{-5}$ m^3 s^{-1} while the analytic flow rate for the rigid tube as obtained from the second equation in Table 2 is $Q_a = 6.62051 \times 10^{-5}$ m^3 s^{-1}.

observe the convergence behavior of the solution with respect to mesh refinement. In all cases we noticed an obvious trend of convergence with improved meshing toward a final solution that does not tangibly improve with further mesh refinement. We also used in these flow simulations a rigid conduit flow model with the same geometry and fluid and flow properties where the flow in the rigid discretized elements was modeled by Poiseuille equation. The purpose of this use of the rigid model is to assess the solution scheme and test its convergence to the correct solution because for Poiseuille-type flow with rigid geometries we have analytical solutions, given in Table 2, that correlate the flow rate to the pressure drop. Poiseuille-type solutions can also provide a qualitative indicator of the sensibility of the distensible solutions; for instance we expect the deviation between the two solutions to decrease with increasing the stiffness of the elastic tube. In all cases the correct quantitative values and qualitative trends have been verified.

Each one of Figs. 3–7 shows a sample of the numeric solutions for two sample meshes used for the distensible flow geometry alongside the converged Poiseuille-type solution for the given fluid and tube parameters. The reason for showing two meshes for the distensible geometry is to demonstrate the convergence behavior with mesh refinement. In all cases, virtually identical solutions were obtained with meshes finer than the finest one shown in these figures.

It should be remarked that in all the distensible flow simulations shown in Figs. 3–7 we used $\alpha = 4/3$ to match the rigid Poiseuille-type flow profile [21] which we used, as indicated already, as a test case. However, for the purpose of testing and validating the distensible model in general we also used

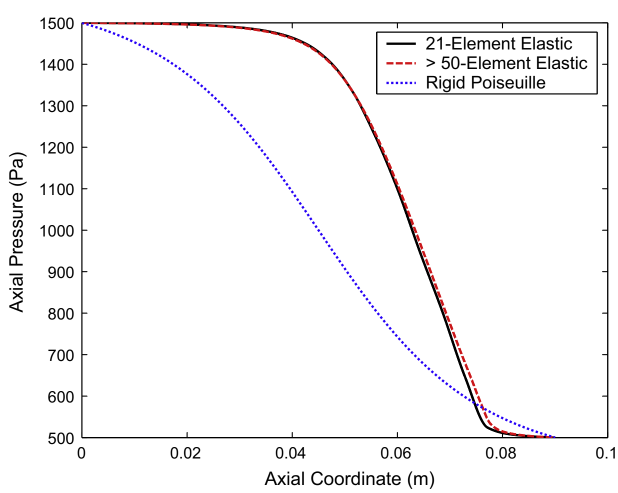

Fig. 5 Axial pressure as a function of axial coordinate for a converging–diverging elastic tube with hyperbolic geometry having $L = 0.09$ m, $R_{min} = 0.004$ m, $R_{max} = 0.006$ m, and $\beta = 23.6$ Pa m. The fluid properties are: $\rho = 800$ kg m^{-3} and $\mu = 0.002$ Pa s while the inlet and outlet pressures are: $p_i = 1500$ Pa and $p_o = 500$ Pa. The Poiseuille-type flow uses a rigid tube with the same unstressed geometry and the same μ and boundary pressures. The converged flow rate for the elastic Navier–Stokes and rigid Poiseuille-type flows are respectively: $Q_e = 0.000147335$ m^3 s^{-1} and $Q_r = 0.000934645$ m^3 s^{-1} while the analytic flow rate for the rigid tube as obtained from the third equation in Table 2 is $Q_a = 0.000933394$ m^3 s^{-1}.

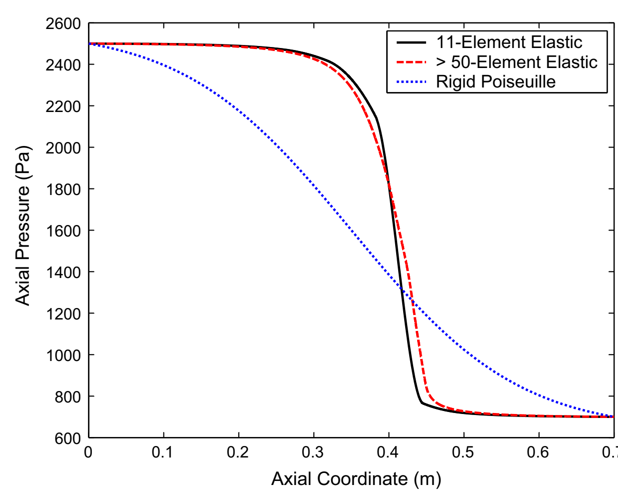

Fig. 6 Axial pressure as a function of axial coordinate for a converging–diverging elastic tube with hyperbolic cosine geometry having $L = 0.7$ m, $R_{min} = 0.05$ m, $R_{max} = 0.08$ m, and $\beta = 3889.4$ Pa m. The fluid properties are: $\rho = 700$ kg m^{-3} and $\mu = 0.0075$ Pa s while the inlet and outlet pressures are: $p_i = 2500$ Pa and $p_o = 700$ Pa. The Poiseuille-type flow uses a rigid tube with the same unstressed geometry and the same μ and boundary pressures. The converged flow rate for the elastic Navier–Stokes and rigid Poiseuille-type flows are respectively: $Q_e = 0.0427687$ m^3 s^{-1} and $Q_r = 1.4184$ m^3 s^{-1} while the analytic flow rate for the rigid tube as obtained from the fourth equation in Table 2 is $Q_a = 1.416296$ m^3 s^{-1}.

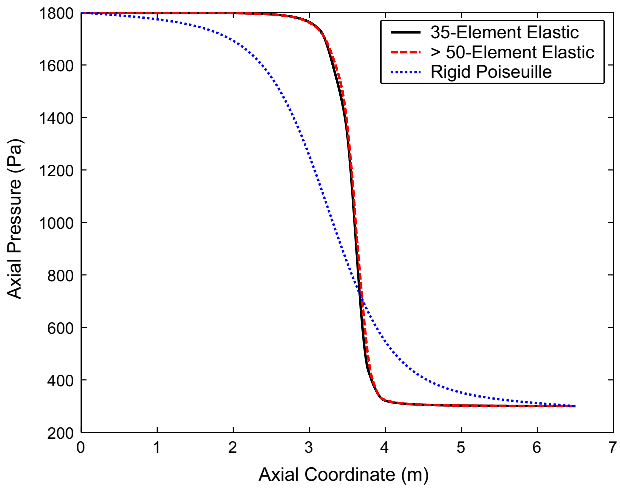

Fig. 7 Axial pressure as a function of axial coordinate for a converging–diverging elastic tube with sinusoidal geometry having $L = 6.5$ m, $R_{min} = 0.2$ m, $R_{max} = 0.5$ m, $\beta = 5064.2$ Pa m. The fluid properties are: $\rho = 900$ kg m^{-3} and $\mu = 0.06$ Pa s while the inlet and outlet pressures are: $p_i = 1800$ Pa and $p_o = 300$ Pa. The Poiseuille-type flow uses a rigid tube with the same unstressed geometry and the same μ and boundary pressures. The converged flow rate for the elastic Navier–Stokes and rigid Poiseuille-type flows are respectively: $Q_e = 0.396769$ m^3 s^{-1} and $Q_r = 8.74955$ m^3 s^{-1} while the analytic flow rate for the rigid tube as obtained from the fifth equation in Table 2 is $Q_a = 8.73370$ m^3 s^{-1}.

an extensive range of values greater than and less than 4/3 for α without observing incorrect convergence or convergence difficulties. In fact using values other than $\alpha = 4/3$ makes the convergence easier in many cases [11].

An interesting feature that can be seen in Fig. 4 is that all the pressure profile curves are almost identical as well as the flow rates. The reason is that, due to the high tube stiffness used in this example, the distensible tube solution converged to the rigid tube Poiseuille-type solution. A more detailed comparison between the Poiseuille-type rigid tube flow and the Navier–Stokes one-dimensional elastic tube flow with high stiffness is shown in Fig. 8 where the results of Figs. 3–7 are reproduced using the same fluid, flow and tube parameters but with high tube stiffness by using large β's. As seen in Fig. 8 the elastic tube flow converges almost identically to the Poiseuille-type rigid tube flow with increasing the tube wall stiffness in all cases. This sensible and correct trend can be regarded as another verification and validation for the residual-based method and the related computer code. Similar results have also been obtained in [47] in comparing the rigid and distensible models for the flow in networks of interconnected straight cylindrical tubes. More detailed comparisons between the rigid and distensible one-dimensional flow models can be found in the aforementioned reference.

It should be remarked that the critical value of β at which the distensible flow solution converges to the rigid flow solution depends on several factors such as the fluid and flow parameters as well as the geometry of the tube and the pressure field regime characterized by the applied boundary conditions at the inlet and outlet where their size and the magnitude of their difference play a decisive role. Another remark is that the shape of the pressure profile curve is highly dependent on the geometric factors such as $\frac{L}{R_{min}}$, $\frac{L}{R_{max}}$, and $\frac{R_{min}}{R_{max}}$ ratios. It also depends on the fluid and tube mechanical properties, such as fluid viscosity and tube wall stiffness, and the magnitude of pressure at the inlet and outlet boundaries.

The opposite to what in Fig. 4 can be seen in Fig. 5 for the hyperbolic geometry where we used very low stiffness and hence the elastic model deviated largely from the rigid model. This also affected the dependency of convergence rate on discretization where the discrepancy between the solutions of the coarse and fine meshes was more substantial than in the other cases for similar coarse and fine meshes. In general, the deviation between the rigid and distensible flow models is maximized by reducing the stiffness, and hence increasing the tube distensibility, while other parameters are kept fixed.

Another interesting feature is that in the flow solution of Fig. 6 there is a big difference between the flow rate of the elastic and rigid tubes. This can be explained largely by the significant deviation from linearity due to the large values of the inlet and outlet boundary pressures, as well as the large size

Table 2 The equations describing the dependency of the flow rate Q on the pressure drop Δp for the rigid tubes with the five converging–diverging geometries of Table 1. These relations were previously [21] derived and validated.

Geometry	$Q(\Delta p)$
Conic	$\frac{3\pi^2\Delta p}{\kappa\rho L}\left(\frac{R_{min}^3 R_{max}^3}{R_{min}^2+R_{min}R_{max}+R_{max}^2}\right)$
Parabolic	$\frac{2\pi^2\Delta p}{\kappa\rho L}\left(\frac{1}{3R_{min}R_{max}^3}+\frac{5}{12R_{min}^2R_{max}^2}+\frac{5}{8R_{min}^3R_{max}}+\frac{5\arctan\left(\sqrt{\frac{R_{max}-R_{min}}{R_{min}}}\right)}{8R_{min}^{7/2}\sqrt{R_{max}-R_{min}}}\right)^{-1}$
Hyperbolic	$\frac{2\pi^2\Delta p}{\kappa\rho L}\left(\frac{1}{R_{min}^2R_{max}^2}+\frac{\arctan\left(\sqrt{\frac{R_{max}^2-R_{min}^2}{R_{min}^2}}\right)}{R_{min}^3\sqrt{R_{max}^2-R_{min}^2}}\right)^{-1}$
Hyperbolic cosine	$\frac{3\pi^2\Delta p}{\kappa\rho L}\left(\frac{\operatorname{arccosh}\left(\frac{R_{max}}{R_{min}}\right)R_{min}^4}{\tanh\left(\operatorname{arccosh}\left(\frac{R_{max}}{R_{min}}\right)\right)\left[\operatorname{sech}^2\left(\operatorname{arccosh}\left(\frac{R_{max}}{R_{min}}\right)\right)+2\right]}\right)$
Sinusoidal	$\frac{16\pi^2\Delta p}{\kappa\rho L}\left(\frac{(R_{max}R_{min})^{7/2}}{2(R_{max}+R_{min})^3+3(R_{max}+R_{min})(R_{max}-R_{min})^2}\right)$

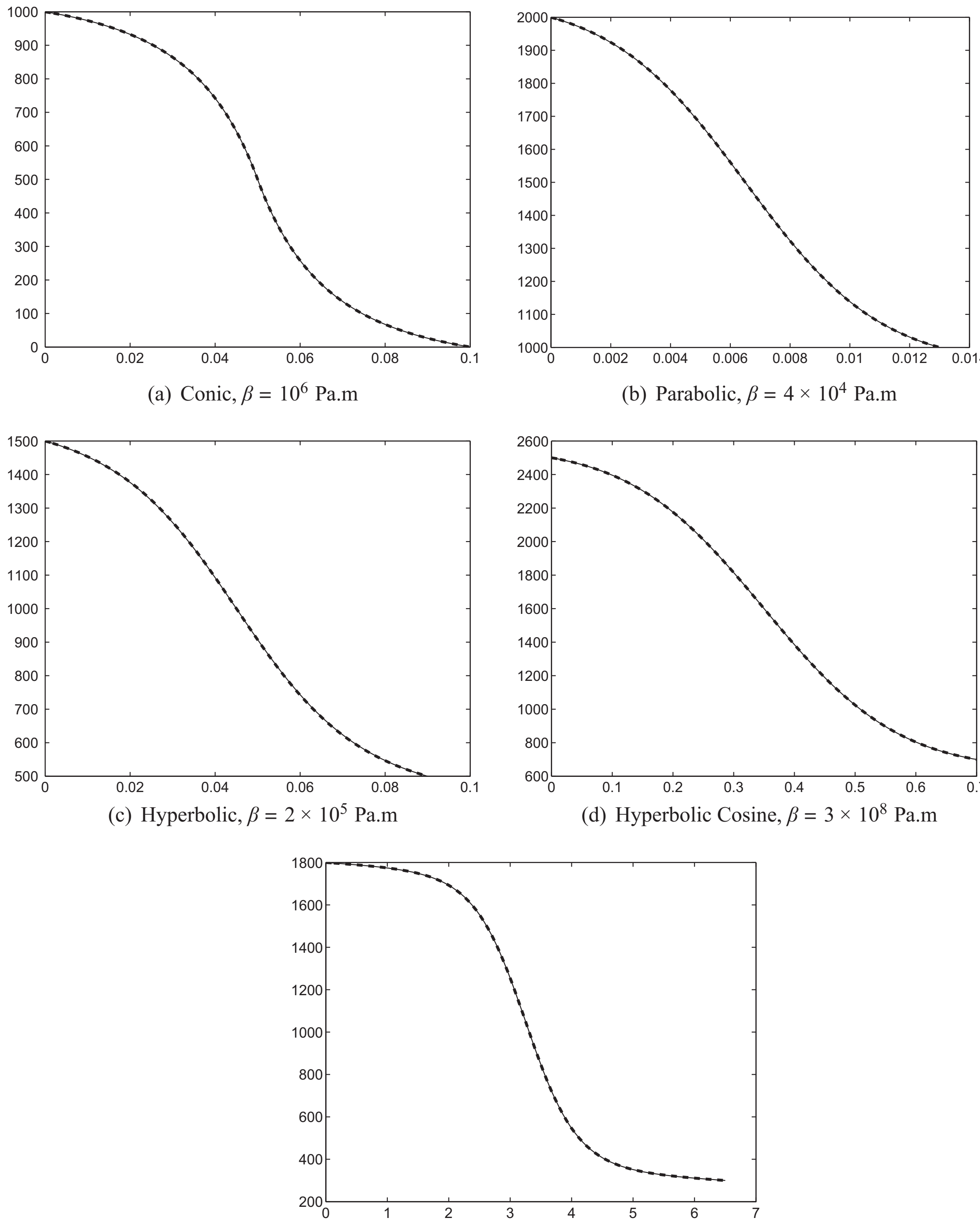

(a) Conic, $\beta = 10^6$ Pa.m

(b) Parabolic, $\beta = 4 \times 10^4$ Pa.m

(c) Hyperbolic, $\beta = 2 \times 10^5$ Pa.m

(d) Hyperbolic Cosine, $\beta = 3 \times 10^8$ Pa.m

(e) Sinusoidal, $\beta = 10^8$ Pa.m

Fig. 8 Comparing the converged Poiseuille-type rigid tube flow (solid) to the converged elastic tube flow with high wall stiffness of the given β (dashed) for the five examples of Figs. 3–7. In all the five sub-figures, the vertical axis represents the axial pressure in pascals while the horizontal axis represents the tube axial coordinate in meters. The converged numeric flow rate in each case for the rigid and elastic models is virtually identical to the corresponding Poiseuille-type analytic flow rate given in Figs. 3–7.

of their difference, with a relatively low stiffness. This indicates that the rigid tube flow model is not a suitable approximation for simulating and analyzing the flow in distensible tubes and networks, as it has been done for instance in some hemodynamic studies. More detailed discussions about this issue can be found in [47].

In Fig. 9 we draw the geometric profile of the elastic tube for the stressed and unstressed states for the five examples of Figs. 3–7 where we plot the tube radius versus its axial coordinate for these two states. As seen, these plots show another sensible qualitative trend in these results and hence provide further endorsement to the residual-based method.

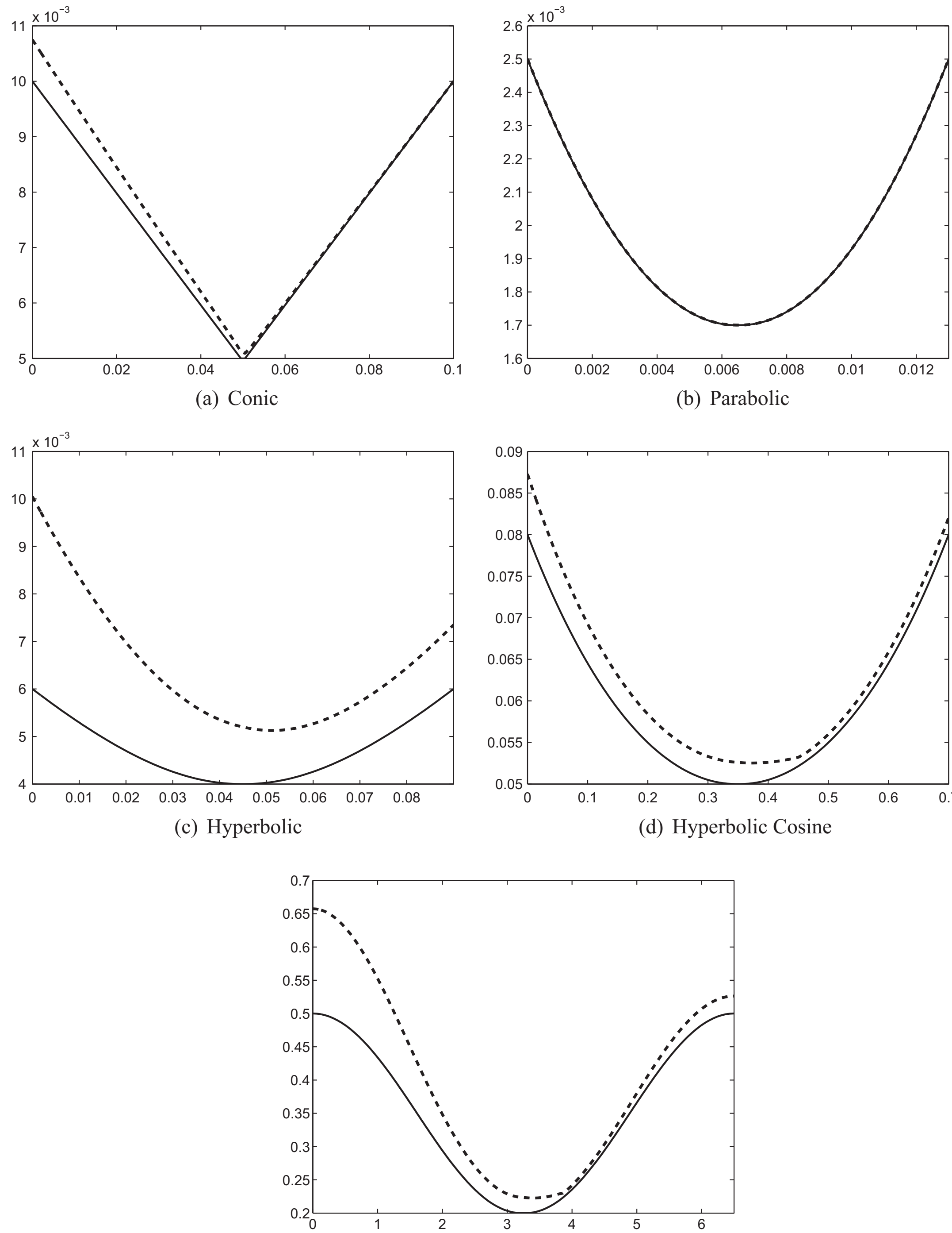

(a) Conic

(b) Parabolic

(c) Hyperbolic

(d) Hyperbolic Cosine

(e) Sinusoidal

Fig. 9 Comparing the elastic tube unstressed radius (solid) to the stressed radius (dashed) as a function of the tube axial coordinate for the five examples of Figs. 3–7. In all the five sub-figures, the vertical axis represents the tube radius in meters and the horizontal axis represents the tube axial coordinate in meters as well.

Finally, it is noteworthy that because the lubrication approximation is based on discretizing the tube into sections each with a constant unstressed radius, the effect of the curvature, especially around the middle of the tube, on the flow is not considered directly. However, as the discretization improves by employing more refined meshes, the effect of curvature will be considered indirectly by the smooth transition from one part of the tube to the next where the difference in radius between any two successive sections will decrease. This can be shown by observing the convergence behavior as a function of the mesh size in Fig. 10 where the percentage difference in Q relative to the solution on the finer mesh size is plotted as a function of the number of discretized sections for a typical hyperbolic geometry example. The plot clearly

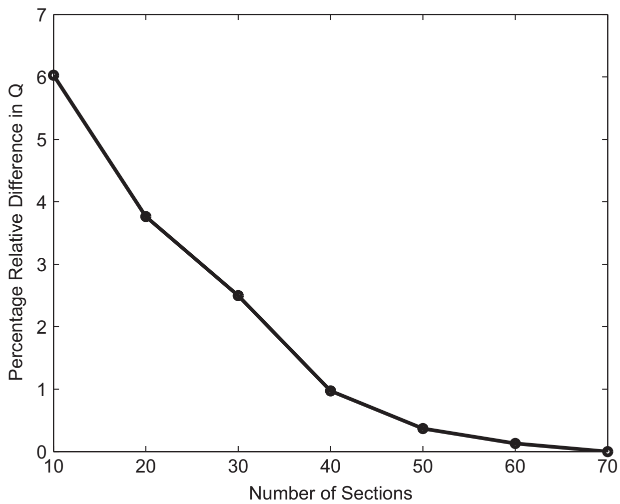

Fig. 10 Percentage difference in Q relative to the solution on the finer mesh size using a hyperbolic geometry with typical fluid and tube properties, as given in Fig. 5.

demonstrates the convergence to a final solution. This convergence behavior suggests that the lubrication solution is improving with increasing the number of sections and hence effects arising from curvature and similar geometric factors are becoming increasingly included.

4. Tests and validations

We used several metrics to validate the residual-based method and check our computer code and flow solutions. First, we did extensive tests on distensible cylindrical tubes with fixed radius using different fluid, flow and tube parameters where the method produced results identical to the analytical flow solutions given by Eq. (5). Although this test is based on a simple limiting case and hence it may be regarded as trivial, it provides sufficient validation for the basic approach and the reliability of the code. We also investigated the convergence behavior, outlined in the previous section, as a function of discretization; in all cases it was observed that the residual-based method converges to a final solution with the use of finer meshes where it eventually stabilizes without tangible change in the solution with more mesh refinement. This convergence behavior is a strong qualitative indicator for the accuracy of the method and the reliability of the code. As indicated previously, we used evenly-divided regular meshes in all simulations.

We also used the discretized Poiseuille-type flow in the same converging–diverging geometry but with rigid wall mechanical characteristics to validate the solutions, as discussed in the previous section. As seen, we observed in all cases the convergence of the Poiseuille-type solutions on using reasonably fine meshes to the analytical solutions with errors that are comparable to the machine precision and hence are negligible as they are intrinsic to any machine-based numerical method. Since the elastic and rigid models are based on the same mathematical and computational infrastructure, the convergence of the rigid flow model to the correct analytical solution can be regarded as an indirect endorsement to the elastic model. The convergence of the elastic model solution to the verified rigid model solution with increasing tube wall stiffness is another indirect support for the elastic model as it demonstrates its sensible behavior.

As another way of test and validation, we produced a sample of lubrication-based one-dimensional finite element solutions which are obtained by discretizing the converging–diverging distensible geometries and applying the pressure continuity, rather than the Bernoulli energy conservation principle, as a coupling condition at the nodal interfaces [27,13] to match the assumptions of the residual-based method which couples the discretized elements by the continuity of pressure condition [11]. The finite element results were very similar to the residual-based results although the convergence behavior was generally different. Broadly, the residual-based method has a better convergence behavior in terms of accuracy and speed as well as other beneficial features like lower computational cost and robustness although this may be dependent on coding technical issues and implementation specificities.

With regard to the comparison between the residual-based and finite element methods, they have very similar theoretical infrastructure as they are both based on the same formulation of the one-dimensional Navier–Stokes flow. In fact the residual-based method is a modified version of the previously proposed [11] pore-scale network modeling method for the flow of Navier–Stokes fluids in networks of interconnected distensible tubes by extending the concept of a network to serially-connected tubes with varying radii which represent the discretized elements of the converging–diverging tubes. Hence the agreement between the residual-based and finite element methods may not be regarded as an entirely independent validation method and that is why we did not do detailed validation by the lubrication-based one-dimensional finite element.

5. Comparisons

As indicated previously, the advantages of the residual-based method in comparison with other methods include simplicity, ease of implementation, low computational costs, and reliability of solutions which are comparable in their accuracy with any intended analytical solutions based on the given assumptions, as the investigated limiting cases like rigid and fixed-radius tubes have revealed. These advantages also apply for the residual-based method in comparison with the lubrication-based one-dimensional finite element method plus a better overall convergence behavior. The biggest advantage of the finite element method, however, is its applicability to the transient time-dependent flow and more suitability for probing other flow-related one-dimensional transport phenomena such as the reflection and propagation of pressure waves. Therefore, the lubrication-based one-dimensional finite element could be the method of choice for investigating transient flow and wave propagation in distensible geometries until proper modifications are introduced on the residual-based method to extend it to these modalities. More details about the comparison between the residual-based and finite element methods can be found in [11].

The residual-based method, as indicated earlier, can also be used for irregular flow conduits in general with cross sections that vary in size and shape and even without converging–diverging feature and regardless of being cylindrically axi-symmetric as long as an analytical, or empirical, or even numerical [43] relation between the boundary pressures and flow rate on a straight geometry with a similar cross-sectional shape does exist. Therefore it can be safely claimed that the residual-based method has a wider applicability range than many other methods whose explicit or implicit underlying assumptions apply only to restricted types of conduit geometry.

With regard to convergence, each numerical method has its own characteristic convergence behavior which depends on many factors such as the utilized numerical solvers and their underlying mathematical and computational theory, the nature of the physical problem, the employed convergence support techniques, and coding technicalities. Hence it is not easy to make a definite comparison for the convergence behavior between different numerical methods. However, we can say that the residual-based method has in general a better rate and speed of convergence in comparison with other commonly-used numerical methods. More details about convergence issues and convergence enhancement techniques can be found in [11].

On the other hand, the residual-based method has a number of limitations based on its underlying physical assumptions, as stated in Section 2, as well as limitations rooted in its one-dimensional nature that restricts its applicability to modeling axially-dependent flow phenomena and hence excludes phenomena related to other types of dependency. However, most of these limitations are shared by other comparable methods.

6. Conclusions

A simple and reliable method based on the lubrication approximation in conjunction with a non-linear simultaneous solution scheme based on the continuity of pressure and volumetric flow rate with an analytical solution correlating the flow rate to the boundary pressures in straight cylindrical elastic tubes with constant radius is used in this paper to find the flow rate and pressure field in distensible tubes with converging–diverging shapes. Five converging–diverging axi-symmetric geometries were used for demonstrating the applicability of the method and assessing its merit.

The method is validated by its convergence behavior with finer discretization as well as comparing the equivalent Poiseuille-based flow to the analytical solutions which were obtained and validated previously. A sample of lubrication-based one-dimensional finite element solutions have also been obtained and compared to the residual-based solutions; these results show very good agreement. The method was also tested on limiting cases of elastic cylindrical tubes with fixed radius, where it produced results identical to the analytical solutions, as well as the convergence to the established rigid tube flow with increasing tube wall stiffness.

The method can be extended to geometries other than cylindrically axi-symmetric converging–diverging shapes as long as a flow characterization relation can be provided for the discretized elements; whether analytical or empirical or even numerical. The method can also be extended beyond the use in computing the flow in single tubes to compute the flow in networks of interconnected distensible conduits which are, totally or partially, characterized by having converging–diverging geometries, or variable cross-sectional shapes or curving structure in the flow direction to be more general.

Many industrial and medical applications, such as material processing and stenosis modeling, can benefit from this approach which is easy to implement and integrate with other flow modeling techniques. Moreover, it produces highly accurate solutions with low computational costs. An initial investigation indicates that its convergence behavior in terms of speed, accuracy and reliability is generally superior to that of the traditional numerical techniques such as the one-dimensional finite element especially with the use of convergence enhancement techniques.

References

[1] J.B. Shukla, R.S. Parihar, B.R.P. Rao, Effects of stenosis on non-Newtonian flow of the blood in an artery, Bull. Math. Biol. 42 (3) (1980) 283–294.

[2] C.D. Han (Ed.), Multiphase Flow in Polymer Processing, first ed., Academic Press, 1981.

[3] D.W. Ruth, H. Ma, Numerical analysis of viscous, incompressible flow in a diverging–converging RUC, Transp. Porous Media 13 (2) (1993) 161–177.

[4] B.B. Dykaar, P.K. Kitanidis, Macrotransport of a biologically reacting solute through porous media, Water Resour. Res. 32 (2) (1996) 307–320.

[5] T. Sochi, Pore-Scale Modeling of Non-Newtonian Flow in Porous Media, PhD Thesis, Imperial College London, 2007.

[6] A. Valencia, D. Ledemann, R. Rivera, E. Bravo, M. Galvez, Blood flow dynamics and fluid-structure interaction in patient-specific bifurcating cerebral aneurysms, Int. J. Numer. Meth. Fluids 58 (10) (2008) 1081–1100.

[7] T. Sochi, Non-Newtonian flow in porous media, Polymer 51 (22) (2010) 5007–5023.

[8] W.G. Gray, C.T. Miller, Thermodynamically constrained averaging theory approach for modeling flow and transport phenomena in porous medium systems: 8. Interface and common curve dynamics, Adv. Water Resour. 33 (12) (2010) 1427–1443.

[9] A. Plappally, A. Soboyejo, N. Fausey, W. Soboyejo, L. Brown, Stochastic modeling of filtrate alkalinity in water filtration devices: transport through micro/nano porous clay based ceramic materials, J. Nat. Environ. Sci. 1 (2) (2010) 96–105.

[10] H.O. Balan, M.T. Balhoff, Q.P. Nguyen, W.R. Rossen, Network modeling of gas trapping and mobility in foam enhanced oil recovery, Energy Fuels 25 (9) (2011) 3974–3987.

[11] T. Sochi, Pore-scale modeling of Navier–Stokes flow in distensible networks and porous media, Comput. Model. Eng. Sci. 99 (2) (2014) 151–168.

[12] T. Sochi, Non-Newtonian Rheology in Blood Circulation, 2014 (submitted for publication). arXiv:1306.2067.

[13] T. Sochi, Fluid flow at branching junctions, Int. J. Fluid Mech. Res. 42 (1) (2015) 59–81.

[14] N. Phan-Thien, C.J. Goh, M.B. Bush, Viscous flow through corrugated tube by boundary element method, J. Appl. Math. Phys. (ZAMP) 36 (3) (1985) 475–480.

[15] N. Phan-Thien, M.M.K. Khan, Flow of an Oldroyd-type fluid through a sinusoidally corrugated tube, J. Nonnewton. Fluid Mech. 24 (2) (1987) 203–220.

[16] S.R. Burdette, P.J. Coates, R.C. Armstrong, R.A. Brown, Calculations of viscoelastic flow through an axisymmetric corrugated tube using the explicitly elliptic momentum equation formulation (EEME), J. Nonnewton. Fluid Mech. 33 (1) (1989) 1–23.

[17] D.F. James, N. Phan-Thien, M.M.K. Khan, A.N. Beris, S. Pilitsis, Flow of test fluid M1 in corrugated tubes, J. Nonnewton. Fluid Mech. 35 (2–3) (1990) 405–412.

[18] S. Huzarewicz, R.K. Gupta, R.P. Chhabra, Elastic effects in flow of fluids through sinuous tubes, J. Rheol. 35 (2) (1991) 221–235.
[19] T. Sochi. The Flow of Newtonian Fluids in Axisymmetric Corrugated Tubes, 2010. arXiv:1006.1515v1.
[20] T. Sochi, The flow of power-law fluids in axisymmetric corrugated tubes, J. Petrol. Sci. Eng. 78 (3–4) (2011) 582–585.
[21] T. Sochi, Newtonian flow in converging–diverging capillaries, Int. J. Model. Simul. Sci. Comput. 04 (03) (2013) 1350011.
[22] S. Miekisz, The flow and pressure in elastic tube, Phys. Med. Biol. 8 (3) (1963) 319.
[23] V.C. Rideout, D.E. Dick, Difference-differential equations for fluid flow in distensible tubes, IEEE Trans. Biomed. Eng. 14 (3) (1967) 171–177.
[24] M. Heil, Stokes flow in an elastic tube – A large-displacement fluid-structure interaction problem, Int. J. Numer. Meth. Fluids 28 (2) (1998) 243–265.
[25] K. Vajravelu, S. Sreenadh, P. Devaki, K.V. Prasad, Mathematical model for a Herschel–Bulkley fluid flow in an elastic tube, Cent. Eur. J. Phys. 9 (5) (2011) 1357–1365.
[26] X. Descovich, G. Pontrelli, S. Melchionna, S. Succi, S. Wassertheurer, Modeling fluid flows in distensible tubes for applications in hemodynamics, Int. J. Mod. Phys. C 24 (5) (2013) 1350030.
[27] T. Sochi, One-Dimensional Navier–Stokes Finite Element Flow Model, Technical Report, 2013. arXiv:1304.2320.
[28] T. Sochi, Navier–Stokes flow in cylindrical elastic tubes, J. Appl. Fluid Mech. 8 (2) (2015) 181–188.
[29] A.J. Greidanus, R. Delfos, J. Westerweel, Drag reduction by surface treatment in turbulent Taylor–Couette flow, J. Phys: Conf. Ser. 318 (8) (2011) 082016.
[30] G.C. Georgiou, G. Kaoullas, Newtonian flow in a triangular duct with slip at the wall, Meccanica 48 (10) (2013) 2577–2583.
[31] K.D. Housiadas, Viscoelastic Poiseuille flows with total normal stress dependent, nonlinear Navier slip at the wall, Phys. Fluids 25 (4) (2013) 043105.
[32] A. Ramachandra Rao, Unsteady flow with attenuation in a fluid filled elastic tube with a stenosis, Acta Mech. 49 (3–4) (1983) 201–208.
[33] A. Ramachandra Rao, Oscillatory flow in an elastic tube of variable cross-section, Acta Mech. 46 (1–4) (1983) 155–165.
[34] P. Chaturani, R. Ponnalagarsamy, Analysis of pulsatile blood flow through stenosed arteries and its applications to cardiovascular diseases, in: Proceedings of the 3rd National Conference on Fluid Mechanics and Fluid Power, 1984, pp. 463–468.
[35] P. Chaturani, R.P. Samy, A study of non-Newtonian aspects of blood flow through stenosed arteries and its applications in arterial diseases, Biorheology 22 (6) (1985) 521–531.
[36] P. Chaturani, R.P. Samy, Pulsatile flow of Casson's fluid through stenosed arteries with applications to blood flow, Biorheology 23 (5) (1986) 499–511.
[37] J.C. Misra, M.K. Patra, Oscillatory flow of a viscous fluid through converging–diverging orthotropic tethered tubes, Comput. Math. Appl. 26 (2) (1993) 87–106.
[38] J. Tambača, S. Čanić, A. Mikelić, Effective model of the fluid flow through elastic tube with variable radius, Grazer Math. Berich. 348 (2005) 91–112.
[39] R. Ponalagusamy, Blood flow through an artery with mild stenosis: A two-layered model, different shapes of stenoses and slip velocity at the wall, J. Appl. Sci. 7 (7) (2007) 1071–1077.
[40] R. Ponalagusamy, R. Tamil Selvi, A.K. Banerjee, Mathematical model of pulsatile flow of non-Newtonian fluid in tubes of varying cross-sections and its implications to blood flow, J. Franklin Inst. 349 (5) (2012) 1681–1698.
[41] R. Ponalagusamy, Mathematical analysis on effect of non-Newtonian behavior of blood on optimal geometry of microvascular bifurcation system, J. Franklin Inst. 349 (9) (2012) 2861–2874.
[42] A. Bucchi, G.E. Hearn, Predictions of aneurysm formation in distensible tubes: Part A – theoretical background to alternative approaches, Int. J. Mech. Sci. 71 (2013) 1–20.
[43] T. Sochi, Using the Euler–Lagrange variational principle to obtain flow relations for generalized Newtonian fluids, Rheol. Acta 53 (1) (2014) 15–22.
[44] A.C.L. Barnard, W.A. Hunt, W.P. Timlake, E. Varley, A theory of fluid flow in compliant tubes, Biophys. J. 6 (6) (1966) 717–724.
[45] T. Sochi, Slip at fluid-solid interface, Polym. Rev. 51 (4) (2011) 309–340.
[46] A. Costa, G. Wadge, O. Melnik, Cyclic extrusion of a lava dome based on a stick-slip mechanism, Earth Planet. Sci. Lett. 337–338 (2012) 39–46.
[47] T. Sochi, Comparing Poiseuille with 1D Navier–Stokes Flow in Rigid and Distensible Tubes and Networks, 2014 (submitted for publication). arXiv:1305.2546.
[48] Y. Damianou, G.C. Georgiou, I. Moulitsas, Combined effects of compressibility and slip in flows of a Herschel–Bulkley fluid, J. Nonnewton. Fluid Mech. 193 (2013) 89–102.